Materials Advances

ROYAL SOCIETY OF CHEMISTRY

COMMUNICATION

View Article Online
View Journal | View Issue

Check for updates

Cite this: *Mater. Adv.*, 2024, 5, 1487

Received 25th August 2023,
Accepted 23rd January 2024

DOI: 10.1039/d3ma00597f

rsc.li/materials-advances

Phase transformation between $CsPbBr_3$ and Cs_4PbBr_6 nanocrystals by a cationic oligomeric ligand and water, and their water resistance†

Norio Saito, *[ab] Akihiro Urayama,[b] Takahiro Takei [a] and Nobuhiro Kumada [a]

This article explores the origin of the significant water resistance of $CsPbBr_3$ nanocrystals passivated by a cationic oligomeric ligand. Ligand exchange and X-ray photoemission spectroscopies indicate that a phase transformation between $CsPbBr_3$ and Cs_4PbBr_6 is induced in the presence of the ligand and water, prolonging the duration of the nanocrystals.

Lead halide perovskite nanocrystals (LHP NCs) and related compounds have been intensively investigated for the last decade. Many articles have reported on their attractive photophysical properties, including a very narrow emission window,[1] near-unity photoluminescence quantum yield,[2] and photocatalytic properties,[3] as well as their potential application to optoelectronic devices.[4] Because of the strong ionicity of LHP NCs, they can easily form surface defects when their surface ionic species dissociate to the solvent phase. However, these surface defects greatly deteriorate the electronic and optical properties of LHP NCs.[5] Hence, the surface defects must be sufficiently passivated to exploit their optoelectronic properties. Surface passivation of LHP NCs with aliphatic surfactants (ligands) is a primary method of improving their colloidal stability and optoelectronic properties. Various ligand molecules such as pairs of aliphatic acids and bases,[6] quaternary alkylammonium halides,[7] phosphonic acids,[8] and zwitterionic ligands[9] have been investigated so far. Recent studies[10] have indicated that some surface-passivating ligands can mediate the crystalline phase transformation from three-dimensional (3D) $CsPbX_3$ NCs to zero-dimensional (0D) Cs_4PbBr_6 or two-dimensional $CsPb_2Br_5$, accompanied by considerable changes in their morphology, a blue-shift of absorption, and improved luminescence properties.

We herein explore a novel surface-passivating ligand for LHP NCs and their crystallization processes. Some of the co-authors have reported the surface passivation of $CsPbBr_3$ NCs using a cationic dimeric (gemini) ligand.[11] These NCs exhibited excellent luminescence performance and prominent stability in water compared to those passivated using conventional ligands such as a pair of oleic acid and oleylamine (OA–OAm) and didodecyldimethylammonium bromide (DDAB).[12] Although gemini ligands containing long methylene spacers are strongly bound to the surfaces of $CsPbBr_3$ NCs *via* two-point adsorption,[11] no clear evidence has been presented so far to account adequately for their remarkable water resistance. This article explores the origin of the water resistance of $CsPbBr_3$ NCs passivated using cationic oligomeric ligands, such as gemini and trimeric ligands (Fig. 1), from the perspectives of ligand engineering and crystal chemistry. We demonstrate repeatable phase transformation between 3D $CsPbBr_3$ and 0D Cs_4PbBr_6, mediated by water and an oligomeric ligand, and discuss the mechanism by which the phase transformation contributes to their chemical stability.

The cationic gemini ligand 1,6-bis(dimethyldodecylammonio)-hexane dibromide, referred to as 12-6-12 from now onwards,[13] and trimeric ligand methyldodecylbis[6-(dimethyldodecylammonio)hexane]ammonium tribromide, denoted as 12-6-12-6-12,[13] were synthesized according to the methods described in the literature (for details, see the ESI†). $CsPbBr_3$ NCs were synthesized by the hot injection method[14] using OA and OAm, followed by purification by conducting centrifugation (13 000 rpm) for 10 min at least three times. Then, the synthesized $CsPbBr_3$ NCs were used in the ligand-exchange procedure.[12] $CsPbBr_3$ NCs (0.7 μM) were

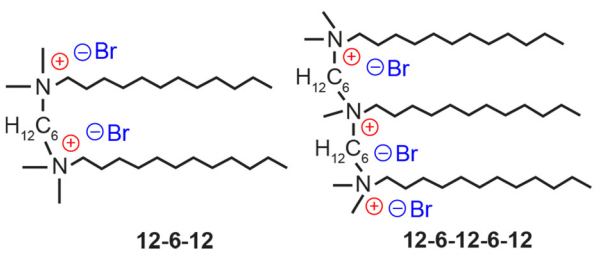

Fig. 1 Molecular structures of 12-6-12 and 12-6-12-6-12.

[a] *Center for Crystal Science and Technology, University of Yamanashi, 7-32 Miyamae, Kofu, Yamanashi 400-8511, Japan. E-mail: n-saito@yamanashi.ac.jp*
[b] *Department of Industrial Chemistry, Faculty of Engineering, Tokyo University of Science, 1-3 Kagurazaka, Shinjuku, Tokyo 162-8601, Japan*

† Electronic supplementary information (ESI) available. See DOI: https://doi.org/10.1039/d3ma00597f

Open Access Article. Published on 24 January 2024. Downloaded on 2/19/2026 7:16:34 PM. This article is licensed under a Creative Commons Attribution-NonCommercial 3.0 Unported Licence.

Open Access Article. Published on 24 January 2024. Downloaded on 2/19/2026 7:16:34 PM. This article is licensed under a Creative Commons Attribution-NonCommercial 3.0 Unported Licence.

agitated in 2.0 mL of toluene containing 0.2 mL of OA and 0.4 mL of DDAB (50 mM), or dichloromethane containing 0.4 mL of 12-6-12 (25 mM) or 12-6-12-6-12 (17 mM). These ligand concentrations are optimal for good NC production; otherwise, the production yield will decrease significantly. After adding 4 mL of ethyl acetate, the precipitate was collected by conducting centrifugation (13 000 rpm) for 10 min and then redispersing it in 3 mL of toluene. Hereafter, the synthesized $CsPbBr_3$ NCs are denoted as $CsPbBr_3$ NCs/"ligand" (*e.g.*, $CsPbBr_3$ NCs/12-6-12).

First, the water resistance of the synthesized $CsPbBr_3$ NCs was tested using the experimental setup reported in our previous article (see details in the ESI†). In this test, 0.5 mL of pure water was added to 2.0 mL of $CsPbBr_3$ NCs, and the mixture was then vigorously stirred. This process accelerated the degradation of $CsPbBr_3$. The yellowish-green solution of $CsPbBr_3$ NCs with an absorbance of 0.5 at 500 nm became white opaque following water exposure for 360 min, when DDAB was used as the passivating ligand (Fig. 2b). However, $CsPbBr_3$ NCs/12-6-12 and 12-6-12-6-12 maintained their green colours (Fig. 2c and d). Powder X-ray diffraction (PXRD) studies on the supernatant obtained after 360 min exposure to water showed that the diffraction patterns of the $CsPbBr_3$ NCs/DDAB exhibited only a strong peak at $2\theta = 29.20^\circ$ corresponding to the 110 diffraction of CsBr, whereas those of $CsPbBr_3$ NCs/12-6-12 and 12-6-12-6-12 exhibited the diffraction of $CsPbBr_3$ (Fig. 2f). Changes in the photoluminescence intensities during the water-resistance test (Fig. 2e) reveal that the relative luminescence intensity of every $CsPbBr_3$ NC except OA–OAm increased by approximately 1.7–1.8 times during the first 120 min due to water insertion into the lattice of $CsPbBr_3$.[15] The luminescence intensities of the $CsPbBr_3$ NCs/12-6-12 and 12-6-12-6-12 were maintained during water exposure for 360 min, in contrast to critical luminescence degradation of $CsPbBr_3$ NCs/OA–OAm and DDAB. These results indicate that the surface passivation using the oligomeric ligands obviously improved the stability of $CsPbBr_3$ NCs toward water exposure.

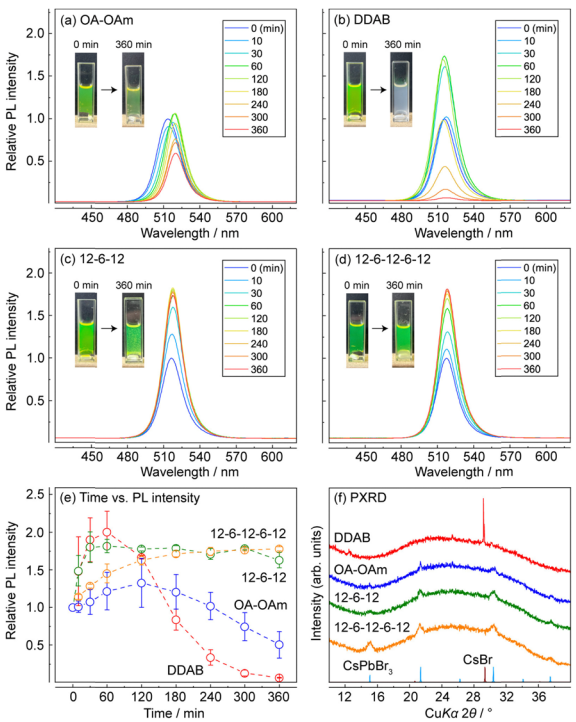

Fig. 2 Results of the water resistance tests: photoluminescence spectra of $CsPbBr_3$ NCs/(a) OA–OAm, (b) DDAB, (c) 12-6-12, and (d) 12-6-12-6-12 during water exposure. (e) Changes in the relative luminescence intensity of $CsPbBr_3$ NCs, and (f) XRD patterns of the supernatants obtained after water exposure for 360 min. The light-blue and dark red patterns show the simulated profiles of $CsPbBr_3$ and CsBr, respectively.

We also evaluated the moisture resistance of dried $CsPbBr_3$ NCs by observing changes in the PXRD patterns of them deposited on a glass XRD holder stored in a 97% relative humidity at 30 °C for several days. The PXRD patterns of $CsPbBr_3$ NCs/OA–OAm (Fig. S1a, ESI†) indicate that the intensities of the diffraction peaks at $2\theta = 11.44^\circ$, 29.18°, and 33.14° sharply increased during exposure to moisture. These peaks are matched with the diffraction pattern of $CsPb_2Br_5$, indicating the degradation of $CsPbBr_3$ to $CsPb_2Br_5$. The PXRD patterns of the ligand-exchanged samples (Fig. S1b–d, ESI†) show that they prevented the degradation to $CsPb_2Br_5$. However, the diffraction peaks corresponding to $CsPbBr_3$ were split and sharpened by exposure to moisture. This indicates an expansion of the lattice volume of $CsPbBr_3$ NCs and their aggregation. Compared to the colloidal NCs, dried ones do not contain free ligand molecules. They are thus likely to aggregate each other. It is speculated that adsorption of water on the surfaces of $CsPbBr_3$ NCs would lead to detachment of the passivating ligands and then cause aggregation of ligand-detached NCs.

The chemical compositions of the synthesized $CsPbBr_3$ NCs were evaluated using a combination of hard X-ray photoemission spectroscopy (HAXPES, $h\nu = 7.939$ keV) and angle-resolved XPS (ARXPS). As the escape depth of the photoelectrons in HAXPES is a few tens of nanometers long, HAXPES is sensitive to the bulk states of the samples. Conversely, ARXPS, which can control the photoelectron escape depth by its take-off angle (TOA, θ), is sensitive to the surface state. The combination of HAXPES and ARXPS can thus clarify the chemical composition of both the surface and bulk states of the samples. Fig. 3 shows the high-resolution HAXPES narrow scans of the Cs 3d, Pb 4f, Br 3p, N 1s, and O 1s regions. As shown in Table S1 (ESI†) listing the binding energies and peak areas of the HAXPES narrow scans determined by peak fitting calculations, the spectral shapes and binding energies of the HAXPES spectra were not significantly varied by the passivating ligand. The atomic concentration of the sample was evaluated from the peak areas of the narrow scans weighted with sensitivity factors.[16] The results of the HAXPES elemental analysis showed that the concentration of Cs:Pb:Br was modified among the passivating ligands (Fig. 4 and Table S1, ESI†). Interestingly, 12-6-12 and 12-6-12-6-12 exhibited a higher concentration of Br and a lower concentration of Pb than that expected by stoichiometry (the stoichiometry of Br and Pb is 60% and 20%, respectively). Thus, the atomic ratio of Br to Pb was higher in these samples. The ARXPS spectra and results of their peak fitting calculations (Fig. S2 and Table S2, respectively, ESI†)

© 2024 The Author(s). Published by the Royal Society of Chemistry

Open Access Article. Published on 24 January 2024. Downloaded on 2/19/2026 7:16:34 PM. This article is licensed under a Creative Commons Attribution-NonCommercial 3.0 Unported Licence.

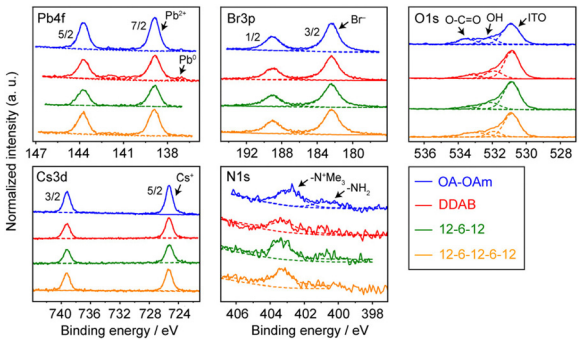

Fig. 3 HAXPES narrow scans of $CsPbBr_3$ NCs/OA–OAm, DDAB, 12-6-12, and 12-6-12-6-12.

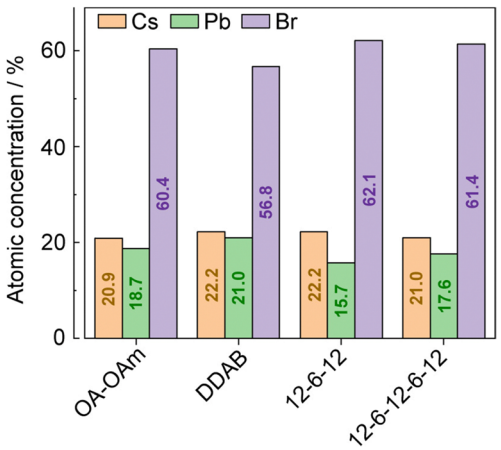

Fig. 4 Atomic concentrations of $CsPbBr_3$ NCs estimated from the peak areas of the HAXPES narrow scans weighted with sensitivity factors.

show that the concentration of Br increased with lower θ. As the photoelectron escape depth in ARXPS is proportional to $\sin\theta$,[17] the abundant Br was present on the surfaces of the $CsPbBr_3$ NCs. On the contrary, the concentration of Cs decreased with lower θ while that of Br and Pb was close to or higher than stoichiometry, suggesting dissociation of the Cs atoms from the NC surface and ligand passivation of the Cs defects.

Fig. S3 (ESI†) shows a Cs–Pb–Br ternary phase diagram that plots the atomic concentrations of $CsPbBr_3$ NCs evaluated by HAXPES. The figure also displays the concentrations for crystallization of ternary compounds estimated from previous literature.[10] These plots demonstrate that the atomic concentrations evaluated by HAXPES are situated on a boundary where a mixture of $CsPbBr_3$ and Cs_4PbBr_6 would crystallize. Considering that the ligand exchange process induced the dissolution of $CsPbBr_3$ NCs and modification of their atomic concentrations, the ligands would influence the crystallization of $CsPbBr_3$, Cs_4PbBr_6, and/or other competitive phase(s).

To examine how the oligomeric ligands influence the crystallization behaviour of the $CsPbBr_3$ NCs, we added excess ligands to the $CsPbBr_3$ NC solution during ligand exchange. The clear green solution became a white opaque suspension with no

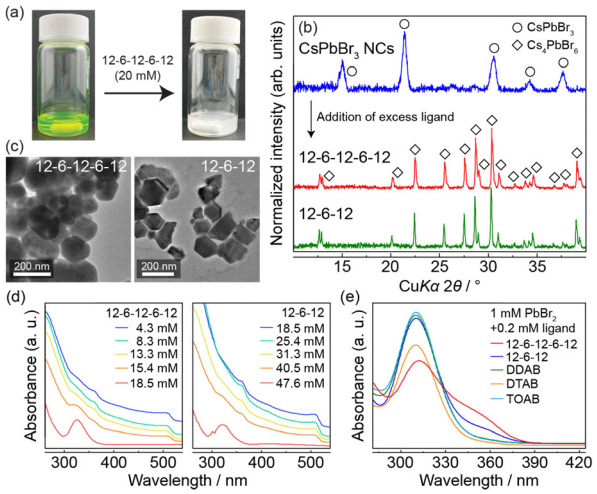

Fig. 5 (a) Photographs of the transformation of the $CsPbBr_3$ NC solution into the white suspension, obtained by adding 12-6-12-6-12 (20 mM). (b) The PXRD patterns of $CsPbBr_3$ NCs and the solids obtained by centrifugation of the suspension obtained using 12-6-12 or 12-6-12-6-12. (c) TEM images of Cs_4PbBr_6 transformed from $CsPbBr_3$ NCs. (d) UV-vis spectra of the $CsPbBr_3$ NC solution containing either 12-6-12-6-12 or 12-6-12. (e) UV-vis spectra of 1.0-mM $PbBr_2$ dissolved in DMF/toluene (1 : 1) solvent containing 0.2-mM 12-6-12-6-12, 12-6-12, DDAB, DTAB, or TOAB.

luminescence (Fig. 5a) when either 12-6-12 or 12-6-12-6-12 was added to the solution until its total concentration exceeded 50 and 20 mM, respectively. The PXRD study of the precipitate obtained by the centrifugation of the suspension indicated that it matched well with the diffraction pattern of Cs_4PbBr_6 (Fig. 5b). The transmission electron microscopy (TEM) images of the obtained Cs_4PbBr_6 show 50–300-nm quasi-spherical or hexagonal particles (Fig. 5c). As its particle size was significantly greater than that of the $CsPbBr_3$ NCs (11–13 nm),[11] the latter were first dissolved and then relatively large Cs_4PbBr_6 was recrystallized. Ultraviolet-visible (UV-vis) spectra of the $CsPbBr_3$ NC solution containing the oligomeric ligand (Fig. 5d) showed that the absorption peaks characteristic of the $CsPbBr_3$ NCs at 505 nm corresponding to the interband transitions gradually weakened with an increase in the concentration of the oligomeric ligand. Moreover, an absorption peak at 325 nm, corresponding to the localized $6S_{1/2}$–$6P_{1/2}$ transitions within the individual $[PbBr_6]^{4-}$ unit in Cs_4PbBr_6, simultaneously appeared.[10] Hence, the UV-vis spectra suggest that the oligomeric ligands induce the dissolution of $CsPbBr_3$ NCs and crystallization of Cs_4PbBr_6. Fig. 5d shows that 18.5 mM of 12-6-12-6-12 transformed almost all $CsPbBr_3$ NCs into Cs_4PbBr_6, which is approximately 0.4 times less than that of 12-6-12 (*i.e.*, 47.6 mM). This result indicates that the trimeric ligand is likely to facilitate the phase transformation.

Notably, the transformation of $CsPbBr_3$ into Cs_4PbBr_6 was not possible with monocationic ligands such as DDAB, dodecyltrimethylammonium bromide (DTAB), and tetraoctylammonium bromide (TOAB). This is because these ligands are not involved in the formation of the multivalent plumbic bromide complex, an essential intermediate in the crystallization of Cs_4PbBr_6. The UV-vis spectra of the 1 : 1 solution of toluene and dimethylformamide (DMF) containing 1-mM $PbBr_2$ and 0.2-mM ligand (Fig. 5e)

Open Access Article. Published on 24 January 2024. Downloaded on 2/19/2026 7:16:34 PM. This article is licensed under a Creative Commons Attribution-NonCommercial 3.0 Unported Licence.

suggest a different behaviour of the plumbic bromide complex among the ligands. The solutions containing either DDAB, DTAB, or TOAB show an absorption peak at 310 nm only, corresponding to the monovalent $[PbBr_3]^-$ complex.[18] In contrast, those containing 12-6-12 or 12-6-12-6-12 exhibited a shoulder-like broad peak at approximately 355 nm corresponding to the divalent $[PbBr_4]^{2-}$ complex.[18] These results suggest that oligomeric ligands, in the presence of Pb^{2+} and Br^- ions, facilitate the formation of plumbate complexes richer in Br than the tribromide ones, which preferentially crystallize in Cs_4PbBr_6 by electrostatic packing with the Cs^+ ions. Although OAm and thiol ligands have been reported to transform $CsPbBr_3$ into Cs_4PbBr_6 because of their coordinating effect on the Pb^{2+} ion,[10] the transformation mechanism for the oligomeric ligands should be different because they repel the metal cation.

Hereafter, we discuss the water resistance of the $CsPbBr_3$ NCs passivated using oligomeric ligands. With respect to water-induced perovskite degradation, Nakamura *et al.* recently clarified that $(CH_3NH_3)PbI_3$ thin films degrade to CH_3NH_3I and PbI_2 under high humidity.[19] Lin *et al.* reported that the structures of the perovskite crystals can be tuned from $CsPbBr_3$ to $CsPb_2Br_5$ by controlling the water-to-dimethylsulfoxide ratios.[20] Accordingly, the possible degradation reactions of $CsPbBr_3$ NCs in contact with water can be assumed as follows:

$$CsPbBr_3 \rightarrow PbBr_2 + CsBr \quad (1)$$

$$2CsPbBr_3 \rightarrow CsPb_2Br_5 + CsBr. \quad (2)$$

Eqn (1) and (2) suggest that the surfaces of $CsPbBr_3$ NCs were exfoliated as either $PbBr_2$ or $CsPb_2Br_5$ when in contact with water because of the dissociation of highly ionic CsBr into the aqueous phase. The resulting plumbic compounds decomposed into plumbic bromide complexes according to the following reactions:

$$PbBr_2 + (Ligand)Br_n + mH_2O \rightarrow (Ligand)[PbBr_{2+n}{\cdot}mH_2O] \quad (3)$$

$$CsPb_2Br_5 + 2(Ligand)Br_n + 2mH_2O \rightarrow 2(Ligand)[PbBr_{2+n}{\cdot}mH_2O] + CsBr, \quad (4)$$

where n and m are the valence number of the surface-passivation ligand and the coordination number of water molecules, respectively. Eqn (3) and (4) indicate that the exfoliated plumbic compounds, ligands, and possibly water molecules form an anionic $[PbBr_{2+n}{\cdot}mH_2O]^{n-}$ complex. Fig. 5e suggests that oligomeric ligands induce the formation of a $[PbBr_4{\cdot}2H_2O]^{2-}$ complex, which could be due to the strong electrostatic interaction between the oligomeric ligand and the divalent anionic complex and the intermolecular interaction of the oligomeric ligands, considering that $[PbBr_4]^{2-}$ is a precursor of lamellar-structured perovskites.[21] We speculated that the Br-rich compositions of $CsPbBr_3$ NCs/12-6-12 and 12-6-12-6-12 observed by HAXPES are due to recrystallization of the Br-rich plumbic complex formed by dissolution of $CsPbBr_3$.

Cs_4PbBr_6 obtained by using excess oligomeric ligand can be changed into an orange solid when water is added to the system. The orange solid was dispersible in toluene and dichloromethane. It exhibited green emission at ~522 nm under UV light (λ = 365 nm), where the wavelength was slightly longer than the as-synthesized samples (Fig. S4, ESI†) due to the larger particle size of the re-formed NCs. The PXRD pattern of the solid (Fig. S5, ESI†) showed the diffraction patterns of the concomitant phases of Cs_4PbBr_6, $CsPbBr_3$, and CsBr, suggesting that Cs_4PbBr_6 partially transformed into $CsPbBr_3$. As discussed in the literature,[22] Cs_4PbBr_6 decomposes into $CsPbBr_3$ by the dissociation of CsBr into the aqueous phase, as follows:

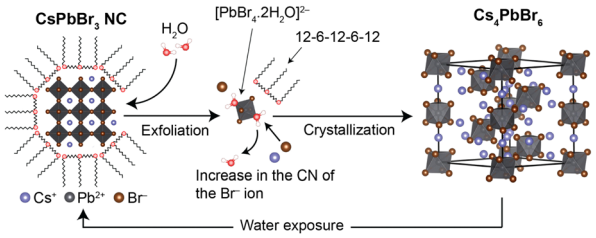

Fig. 6 Schematic illustration of crystalline phase transformation between $CsPbBr_3$ and Cs_4PbBr_6, mediated by 12-6-12-6-12 and water.

$$Cs_4PbBr_6 \rightarrow CsPbBr_3 + 3CsBr. \quad (5)$$

Interestingly, the addition of oligomeric ligands to the $CsPbBr_3$/Cs_4PbBr_6-dispersed solution resulted in the re-transformation of Cs_4PbBr_6 (Fig. S5, ESI†). This result suggests that repeatable phase transformation between $CsPbBr_3$ and Cs_4PbBr_6 is possible with an oligomeric ligand and water (Fig. 6). Note that the luminescence intensity is not fully maintained during the phase transformation due to the dissociation of CsBr into the aqueous phase. However, the oligomeric ligand plays a role not only in protecting the surfaces of $CsPbBr_3$ NCs, but also in recovering their luminescence properties from their degraded states. Hence, it can be concluded that these characteristics contribute to the high chemical stability of oligomeric ligand-passivating perovskite NCs.

In summary, we demonstrated a repeatable transformation between $CsPbBr_3$ and Cs_4PbBr_6 mediated by oligomeric ligands and water. This phenomenon is characteristic of oligomeric ligands because of their affinity for multivalent anions. The oligomeric ligands investigated in this study can be used as efficient passivation agents to improve the chemical stability of perovskite NCs and thin films that can be applied to photovoltaic solar cells and electronic luminescent devices.

Conflicts of interest

There are no conflicts to declare.

Acknowledgements

This work was partly supported by JSPS KAKENHI (grant numbers 21K14706 and 23K04888), a research grant from the Murata Science Foundation (grant number AN20030), and research grants from the Iketani Science, Technology Foundation

© 2024 The Author(s). Published by the Royal Society of Chemistry

Open Access Article. Published on 24 January 2024. Downloaded on 2/19/2026 7:16:34 PM. This article is licensed under a Creative Commons Attribution-NonCommercial 3.0 Unported Licence.

(grant number 0341150-A) and the Nippon Sheet Glass Foundation. The HAXPES measurements were performed at the Japanese synchrotron radiation facility, SPring-8, with non-proprietary approval from the Japan Synchrotron Radiation Research Institute (JASRI) (Proposal numbers 2021B1852/BL46XU and 2022A1758/BL46XU).

References

1 F. Zhang, H. Zhong, C. Chen, X.-G. Wu, X. Hu, H. Huang, J. Han, B. Zou and Y. Dong, *ACS Nano*, 2015, **9**, 4533.
2 L. Protesescu, S. Yakunin, M. I. Bodnarchuk, F. Krieg, R. Caputo, C. H. Hendon, R. X. Yang, A. Walsh and M. V. Kovalenko, *Nano Lett.*, 2015, **15**, 3692; H. Huang, F. Zhao, L. Liu, F. Zhang, X.-G. Wu, L. Shi, B. Zou, Q. Pei and H. Zhong, *ACS Appl. Mater. Interfaces*, 2015, **7**, 28128.
3 H. Huang, B. Pradhan, J. Hofkens, M. B. J. Roeffaers and J. A. Steele, *ACS Energy Lett.*, 2020, **5**, 1107; J. Yuan, H. Liu, S. Wang and X. Li, *Nanoscale*, 2021, **13**, 10281.
4 J. Liu, Y. Xue, Z. Wang, Z.-Q. Xu, C. Zheng, B. Weber, J. Song, Y. Wang, Y. Lu, Y. Zhang and Q. Bao, *ACS Nano*, 2016, **10**, 3536; T. Chiba, S. Ishikawa, J. Sato, Y. Takahashi, H. Ebe, S. Ohisa and J. Kido, *Adv. Opt. Maters.*, 2020, **8**, 2000289; Y.-H. Kim, C. Wolf, Y.-T. Kim, H. Cho, W. Kwon, S. Do, A. Sadhanala, C. G. Park, S.-W. Rhee, S. H. Im, R. H. Friend and T.-W. Lee, *ACS Nano*, 2017, **11**, 6586.
5 D. Yang, X. Li and H. Zeng, *Adv. Mater. Interfaces*, 2018, **5**, 1701662; D. P. Nenon, K. Pressler, J. Kang, B. A. Koscher, J. H. Olshansky, W. T. Osowiecki, M. A. Koc, L.-W. Wang and A. P. Alivisatos, *J. Am. Chem. Soc.*, 2018, **140**, 17760.
6 A. Pan, B. He, X. Fan, Z. Liu, J. J. Urban, A. P. Alivisatos, L. He and Y. Liu, *ACS Nano*, 2016, **10**, 7943; Z. Liang, S. Zhao, Z. Xu, B. Qiao, P. Song, D. Gao and X. Xu, *ACS Appl. Mater. Interfaces*, 2016, **8**, 28824.
7 J. H. Park, A.-Y. Lee, J. C. Yu, Y. S. Nam, Y. Choi, J. Park and M. H. Song, *ACS Appl. Mater. Interfaces*, 2019, **11**, 8428.
8 B. Zhang, L. Goldoni, J. Zito, Z. Dang, G. Almeida, F. Zaccaria, J. W. I. Infante, L. D. Trizio and L. Manna, *Chem. Mater.*, 2019, **31**, 9140.
9 F. Krieg, S. T. Ochsenbein, S. Yakunin, S. Brinck, P. Aellen, A. Süess, B. Clerc, D. Guggisberg, O. Nazarenko, Y. Shynkarenko, S. Kumar, C.-J. Shih, I. Infante and M. V. Kovalenko, *ACS Energy Lett.*, 2018, **3**, 641.
10 Q. Jing, Y. Xu, Y. Su, X. Xing and Z. Lu, *Nanoscale*, 2019, **11**, 1784; Y. Li, H. Huang, Y. Xiong, S. V. Kershaw and A. L. Rogach, *CrystEngComm*, 2018, **20**, 4900; S. K. Balakrishnan and P. V. Kamat, *Chem. Mater.*, 2018, **30**, 74; F. Palazon, G. Almeida, Q. A. Akkerman, L. D. Trizio, Z. Dang, M. Prato and L. Manna, *Chem. Mater.*, 2017, **29**, 4167; Z. Liu, Y. Bekenstein, X. Ye, S. C. Nguyen, J. Swabeck, D. Zhang, S.-T. Lee, P. Yang, W. Ma and A. P. Alivisatos, *J. Am. Chem. Soc.*, 2017, **139**, 5309.
11 N. Saito, A. Urayama, M. Ikezawa and Y. Kondo, *Adv. Mater. Interfaces*, 2022, **9**, 2101836.
12 J. Pan, L. N. Quan, Y. Zhao, W. Peng, B. Murali, S. P. Sarmah, M. Yuan, L. Sinatra, N. M. Alyami, J. Liu, E. Yassitepe, Z. Yang, O. Voznyy, R. Comin, M. N. Hedhili, O. F. Mohammed, Z. Hong Lu, D. H. Kim, E. H. Sargent and O. M. Bakr, *Adv. Mater.*, 2016, **28**, 8718.
13 E. Alami, G. Beinert, P. Marie and R. Zana, *Langmuir*, 1993, **9**, 1465; R. Zana, *J. Colloid Interface Sci.*, 2002, **248**, 203; R. Zana, H. Levy, D. Papoutsi and G. Beinert, *Langmuir*, 1995, **11**, 3694; M. In and V. Bec, *Langmuir*, 2000, **16**, 141.
14 M. I. Bodnarchuk, S. C. Boehme, S. Brinck, C. Bernasconi, Y. Shynkarenko, F. Krieg, R. Widmer, B. Aeschlimann, D. Günther, M. V. Kovalenko and I. Infante, *ACS Energy Lett.*, 2019, **4**, 63; C. K. Ng, C. Wang and J. J. Jasieniak, *Langmuir*, 2019, **35**, 11609.
15 M. Kim, J. H. Kim, M. Kim, C. S. Kim, J. W. Choi, K. Choi, J. H. Lee, J. Park, Y.-C. Kang, S.-H. Jin and M. Song, *J. Ind. Eng. Chem.*, 2020, **88**, 84.
16 J. J. Yeh and I. Lindau, *At. Data Nucl. Data Tables*, 1985, **32**, 1.
17 T. Schneider, K. Artyushkova, J. E. Fulghum, L. Broadwater, A. Smith and O. D. Lavrentovich, *Langmuir*, 2005, **21**, 2300.
18 S. J. Yoon, K. G. Stamplecoskie and P. V. Kamat, *J. Phys. Chem. Lett.*, 2016, **7**, 1368; M. Liu, J. Zhao, Z. Luo, Z. Sun, N. Pan, H. Ding and X. Wang, *Chem. Mater.*, 2018, **30**, 5846.
19 Y. Nakamura, N. Shibayama, K. Fujiwara, T. Koganezawa and T. Miyasaka, *ACS Mater. Lett.*, 2022, **4**, 2409.
20 Q. Lin, S. Bernardi, B. Shabbir, Q. Ou, M. Wang, W. Yin, S. Liu, A. S. R. Chesman, S. O. Fürer, G. Si, N. Medhekar, J. Jasieniak, A. Widmer-Cooper, W. Mao and U. Bach, *Adv. Funct. Maters.*, 2022, **32**, 2109442.
21 M. C. Weidman, M. Seitz, S. D. Stranks and W. A. Tisdale, *ACS Nano*, 2016, **10**, 7830.
22 L. Wu, H. Hu, Y. Xu, S. Jiang, M. Chen, Q. Zhong, D. Yang, Q. Liu, Y. Zhao, B. Sun, Q. Zhang and Y. Yin, *Nano Lett.*, 2017, **17**, 5799; D. Lu, A. Urayama and N. Saito, *Colloids Surf., A*, 2022, **648**, 129345.

© 2024 The Author(s). Published by the Royal Society of Chemistry